Numerical Simulation with the NCAR Global Circulation Model of the Mean Conditions During the Asian-African Summer Monsoon

W. M. WASHINGTON AND S. M. DAGGUPATY[1]

National Center for Atmospheric Research,[2] Boulder, Colo. 80303

(Manuscript received 1 August 1974; in revised form 15 November 1974)

ABSTRACT

A global circulation model (GCM) developed at the National Center for Atmospheric Research (NCAR) has been used to simulate the large-scale features of the Asian-African summer monsoon. The model has 6 vertical layers of 3-km thickness with a 2½° horizontal latitude-longitude grid. The physical processes incorporated are solar and infrared radiation, with cloudiness explicitly calculated from a model-generated relative humidity distribution. The latent heat released from precipitation is derived from stable lifting and cumulus convection. Also included in the model are subgrid-scale vertical and horizontal transports of momentum, sensible heat, and latent heat.

We compare the computed sea-level pressure, wind, cloudiness, and precipitation patterns with observed data and, in particular, concentrate on the strong low-level monsoon jet near eastern Kenya and Somalia. The model correctly simulates this jet in position; however, the wind maxima are weaker than observed. Because of the relatively coarse model resolution, we fail to obtain the important monsoon depressions which form in the Bay of Bengal or near Bombay. In nature, these depressions account for a large part of the precipitation in India and its surrounding regions.

This study demonstrates that a global circulation model is capable of simulating many of the features observed in the Asian-African summer monsoon.

1. Introduction

This paper compares a global circulation model (GCM) simulation of the mean conditions during the Asian-African summer monsoon with observed data. Several numerical models have recently been used to study the features of the Asian-African summer monsoon. For example, Washington (1970) carried out general circulation model experiments with a 5° latitude-longitude grid version of the NCAR model which successfully simulated the cross-equatorial flow in the West Indian Ocean, the low-level westerly flow in the vicinity of India, and the tropical easterly jet (TEJ). The precipitation pattern in this early experiment was incorrect over land areas, particularly Arabia, because of the assumption that all land surfaces were saturated. This saturation assumption restriction has since been removed from the NCAR model and replaced with a ground hydrology parameterization (Washington, 1974) allowing for variable soil moisture. Murakami *et al.* (1970) and Godbole (1973) performed several experiments with a model invoking zonally symmetric equations and applying mean conditions at 80°E. Even without zonal asymmetry, they were able to simulate the principal areas of easterlies and westerlies in cross-sections. Alyea (1972) used a quasi-geostrophic model to simulate the July three-dimensional flow patterns for the Northern Hemisphere. In many aspects, the Alyea model failed to properly simulate the tropical and subtropical flows. The exact reasons for the failure are not known; however, Abbott (1973), using a model similar to Alyea's, generated a monsoon circulation much closer to reality. This leads us to speculate that Alyea's *heating* possibly was the cause of the poor simulation rather than the restrictions implied in the use of quasigeostrophic models vs primitive equation models.

Krishnamurti *et al.* (1973) used the simple barotropic and nondivergent vorticity equation on the beta-plane to experiment with the effect of the Tibetan High treated as a mechanical barrier in the 200-mb flow. With this simple model, they were able to simulate the Mexican High, mid-Atlantic and mid-Pacific troughs, the African High, and the TEJ. This experiment suggests the dominant role that the Tibetan High plays as a barrier in the summer Northern Hemisphere dynamics. Manabe *et al.* (1974) performed a seasonal variation of the tropical circulation with the Geophysical Fluid Dynamics Laboratory (GFDL) model. The simulated wind flow at the lower and higher levels agreed quite well with the observed data. They analyzed principally the seasonal changes in rainfall and ener-

[1] Now with Dynamic Prediction Research Division, Atmospheric Environment Service, Dorval, Quebec, Canada.

[2] The National Center for Atmospheric Research is sponsored by the National Science Foundation.

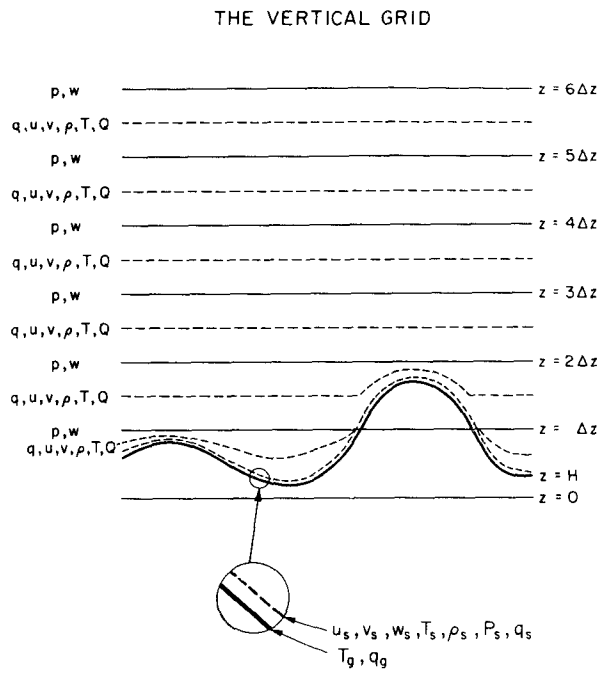

FIG. 1. Vertical grid structure for the 6-layer model with orography.

getics rather than a detailed comparison with observed data of the Asian-African summer monsoon itself.

Here we show simulation results generated by the NCAR model and compare them with observed data of sea-level pressure, wind, cloudiness, and precipitation patterns in the Asian-African summer monsoon region. We find that the basic wind structure in the lower and upper troposphere is correctly simulated, but the wind speed in the TEJ is underestimated. The low-level wind maxima in the observed data appear over small regions and probably are not adequately resolved by the horizontal latitude-longitude grid of $2\frac{1}{2}°$ and the vertical grid of 3 km used in this study. We also note that the small-scale transient systems (of the order of 5°) are not resoluble in the model because of its limited resolution. The presence of strong small-scale transient systems, of course, is quite important for day-to-day weather in the monsoon region, but may not be too essential for a successful simulation of large-scale aspects of the Asian-African summer monsoon. An example of such a transient is the monsoon depressions which move northwest from the Bay of Bengal. These types of depressions have an average frequency of 1.8 per month (Ramage, 1971, p. 45), but it is not unusual to have a higher frequency over a shorter period of time. Monsoon depressions account for approximately 75% of the rainfall over interior India. Because of their size, they are not properly resolved with the $2\frac{1}{2}°$ horizontal grid used in this study.

The strong low-level jets observed near Somalia and Asia are shown in the simulated cross sections. These jets are an extremely interesting feature of the summer monsoon circulation and their dynamics is basically unknown.

2. Model description

We use the $2\frac{1}{2}°$ latitude-longitude version of the NCAR GCM with 6 vertical layers of 3-km height increment (Δz) each. The vertical grid is shown in Fig. 1 where pressure p and vertical velocity w are computed at the ground, 3, 6, . . ., 18 km, and u and v horizontal wind components, temperature T, specific humidity q, density ρ and heating and cooling Q are computed at 1.5, 4.5, . . ., 16.5 km; these latter quantities represent layer averages. The variables with subscript s are computed in the boundary layer and those with subscript g at the earth's surface. The orography in this experiment is appropriately smoothed so that it is consistent with the $2\frac{1}{2}°$ horizontal resolution. Features like the Western Ghats, in reality 0.5 to 1.0 km, are smoothed to 0.5 km. The physical processes in the model are solar and infrared radiation, cloudiness calculated at 3 and 9 km from the relative humidity distribution, and horizontal and vertical diffusion of sensible heat, moisture, and momentum.

For the particular experiment described, we use a cumulus convective parameterization developed by Krishnamurti and Moxim (1971). Some preliminary results with this cumulus parameterization scheme compared to the convective adjustment scheme are discussed in Washington and Baumhefner (1974).

The method of cumulus parameterization used in this paper was developed by Kuo (1965) and later modified by Krishnamurti and Moxim (1971). M. Kanamitsu, a student visitor from Florida State University, adapted this method to the NCAR general circulation model. The heating rate due to cumulus convection in the Kuo scheme is

$$Q_c=\frac{ac_p(T_a-T)}{\Delta\tau} \tag{1}$$

where Q_c is the heating rate per unit mass, a is a parameter related to the area covered by cumulus convection, $\Delta\tau$ the lifetime of convection (assumed to be 30 minutes), c_p the specific heat at constant pressure, T_a the temperature along a moist adiabat and T the model temperature. The quantity a is defined as

$$a=\frac{I}{S}, \tag{2}$$

where I is the net convergence of moisture in an air column extending from the cloud base z_b to the cloud top z_c, i.e.,

$$I=-\int_{z_b}^{z_c}\nabla\cdot\rho q\mathbf{V}dz-\rho_c q_c w_c+\rho_b q_b w_b. \tag{3}$$

The variables in (3) are density ρ, specific humidity q, horizontal wind vector $\mathbf{v}$, vertical velocity w; subscripts c and b refer to the top and bottom of the cloud, respectively. In the present formulation in the NCAR model, we assume that the first two terms on the right of (3) are negligible compared to the third. The denominator of (2) is the amount of energy needed to saturate the entire grid volume. For our model, S takes the form

$$S=\frac{1}{\Delta\tau}\int_{z_b}^{z_c}\left[\frac{c_p}{L}(\rho_a T_a-\rho T)+(\rho_a q_a-\rho q)\right]dz, \quad (4)$$

where L is the latent heat of condensation.

The rate of moisture transport by cumulus clouds is

$$\frac{d(\rho q)}{dt}=\frac{a}{\Delta\tau}(\rho_a q_a-\rho q). \quad (5)$$

We assume that all moisture for the cumulus heating and moisture transport comes from the bottom layer of the model. In addition to the convective heating rate, we allow for stable condensation heating whenever the model generates relative humidities in excess of 95%. From experimentation, the original scheme proposed by Kuo seems to underestimate the precipitation in the tropics. We have tried to remedy this shortcoming by making a equal to 1 if the lower layers become supersaturated. Another change having a large effect on the simulation is to increase the vertical eddy diffusion K to values of the order of 10^7 cgs whenever the lower layers become supersaturated. The increased K has the beneficial effect of drying out the lower layers by increasing moisture transport as well as increasing transports of momentum and sensible heat in regions of active condensation.

For a complete description of the physical processes and previous examples of model simulation, see Kasahara and Washington (1967, 1971), Washington (1970) and Washington and Kasahara (1970). Details of the ground hydrologic processes, such as snow cover and soil moisture prediction equations, can be found in Washington (1974). The experiment starts from an isothermal atmosphere over the entire globe with climatological sea-surface temperatures at rest for a perpetual July, and we use Days 91 through 120 for the time means.

3. Comparison of computed low- and high-level wind patterns with observed data

We compare the observed and computed low- and high-level wind patterns in Figs. 2 and 3. The observed mean July winds for 850 and 200 mb for the Asian-African regions are obtained from Ramage and Raman (1972) and Wright and Stubbs (1971).

Since our model has height as a vertical coordinate, we use the nearest levels to the observed—1.5 and 13.5 km. In the low levels (Fig. 2), we are able to simulate the basic low-level easterlies south of the equator which curve near the east coast of Africa and then become westerlies near India. The isotach pattern shows that we can simulate the jet near Somalia and the minimum wind speed over the central Indian Ocean. Because this region is of particular interest, we discuss it in more detail in Section 4. The computed flow into interior East Africa appears to disagree with the observed prepared by Ramage and Raman, but agrees with the studies of Wright and Stubbs. The computed low-level wind maximum in the Bay of Bengal is too far south and a mean monsoon trough across northern India south of the Himalayas fails to form. One possible reason is lack of resolution in orographic features. We also note that the model develops easterlies near Japan which are not in the observed.

In the upper layers (Fig. 3), the model generates anticyclonic centers close to the right longitudes near 30°N with a broad belt of easterlies across the equator to 10°S. The strength of the maximum in the TEJ is underestimated by a factor of 3 and fails to obtain a northerly component as seen in the observed. Possible reasons for a weaker-than-normal TEJ are: a) upper boundary conditions of zero vertical velocity at 18 km, b) lack of ozone heating, or c) misplaced latent heat release (Section 6). We also note that the computed westerlies in the Southern Hemisphere are too far equatorward. The westerlies in both hemispheres are weaker than observed.

4. Low-level cross-equatorial flow

A remarkable feature of the Indian Monsoon is the strong cross-equatorial flow along the east coast of Africa. This feature is quite persistent throughout the entire monsoon season and has been well documented, e.g., Findlater (1969) and, more recently, van de Boogaard (private communication). To compare the computed and observed features in detail, we have taken a 30-day mean cross section along the equator from 35–75°E and from the earth's surface to 5 km. The data of Findlater and van de Boogaard have been replotted for easier comparison with the computed winds in Fig. 4. The two observed sources have the same basic features except for the level where southerlies change to northerlies. The exact reason for the difference in observed data is not known except that they probably covered different time periods. As mentioned earlier, the NCAR model used for this experiment has 3-km vertical layers and a $2\frac{1}{2}°$ horizontal grid so that the computed results will be much smoother than the observed. Even though we obtain the proper location of the jet, we find that the central speed of the computed jet is much too small. Nevertheless, even with the resolution shortcoming of the model, we are able to simulate this feature reasonably well. An additional factor to be considered is that the details of the orog-

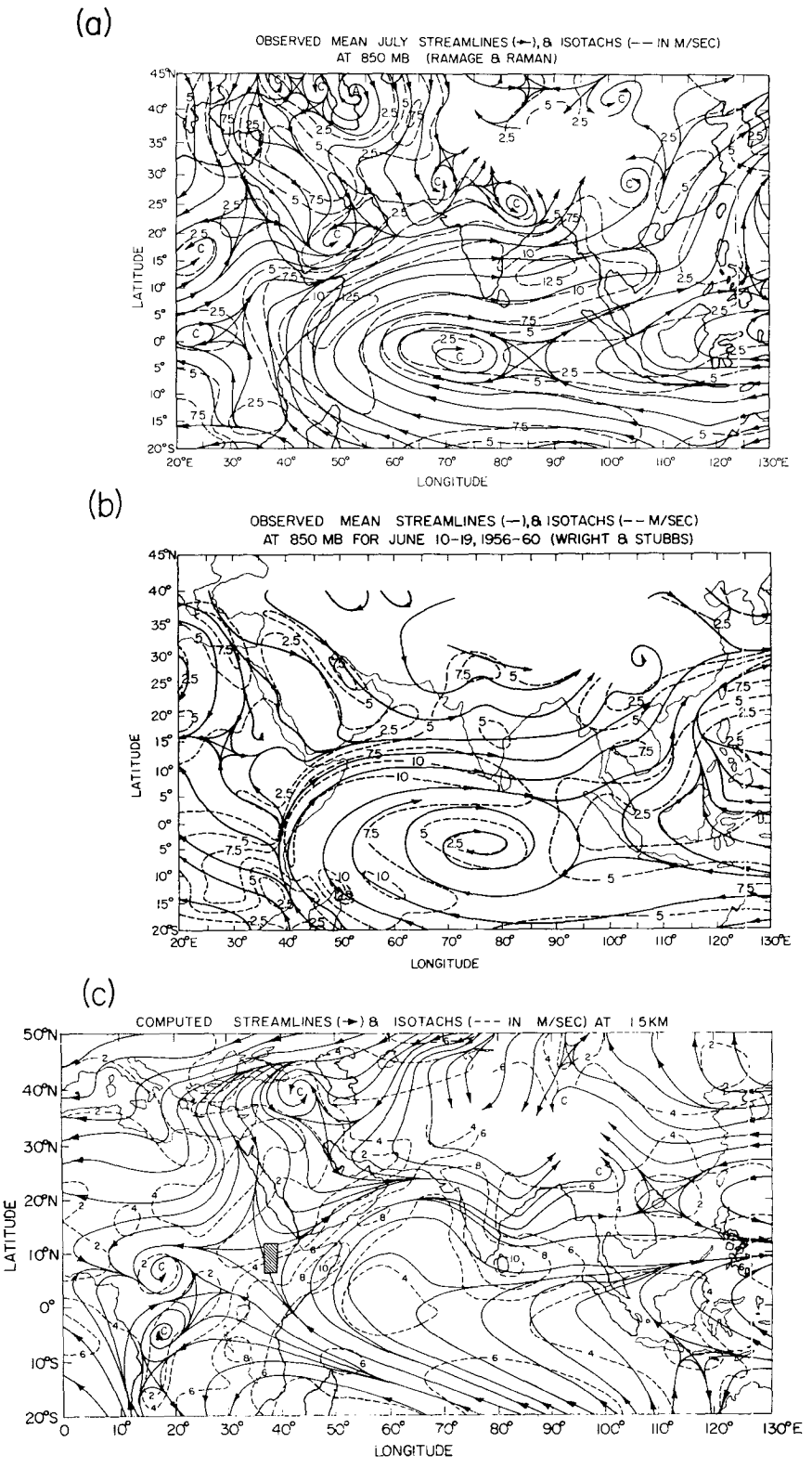

FIG. 2. Observed and computed mean July low-level streamlines and isotachs. (a) 850 mb (Ramage and Raman, 1972); (b) 850 mb (Wright and Stubbs, 1971). (c) Computed at 1.5 km. Units are m s^{-1}. Orographic blocking is shaded.

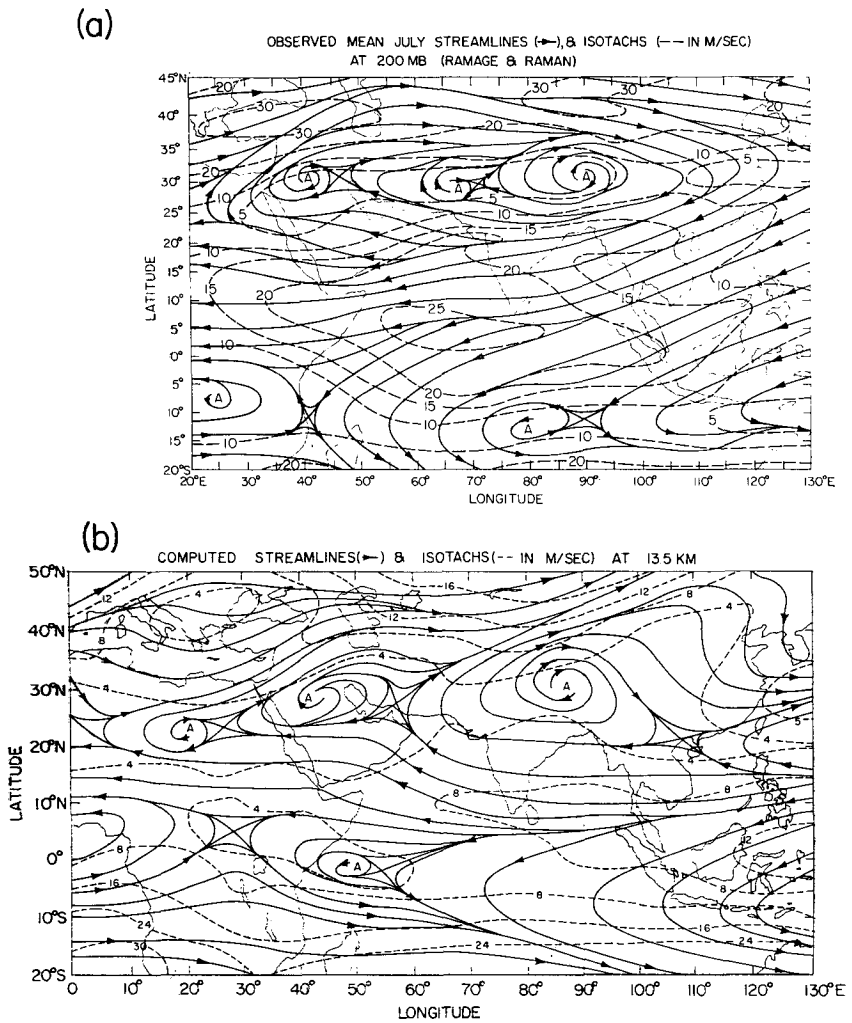

FIG. 3. Observed and computed mean July upper-level streamlines and isotachs. (a) 200 mb (Ramage and Raman, 1972). (b) Computed at 13.5 km. Units are m s^{-1}.

raphy used in the model differ from reality because of smoothing on a $2\frac{1}{2}°$ grid scale; this may also influence the position of the jet.

Figure 5 is a horizontal view of this low-level flow. For the observed source, we use Findlater (1970, 1971) who shows the July monthly mean airflow at 1 km over the western portion of the Indian Ocean. The heavy streamline shows the axis of maximum flow, and the isotachs in 2.5 m s^{-1} intervals are also plotted; the dashed line is a region of minimum wind speed. A similar plot at 1.5 km is given for the computed results. We see many of the same general features in the model results—in particular, the position of the jet maximum over eastern Kenya and Somalia, as well as the turning of the jet maximum south of the equator near Malagasy. The simulated isotach maximum in this same region is too small in the core when compared to Findlater data but agrees well with Ramage and Raman in Fig. 2. We also find that the computed jet appears too far north in the Arabian Sea.

The splitting of flow near Kenya is not shown in the Findlater data, but can be found in the studies of mean winds by Wright and Stubbs (1971) (see Fig. 2) and Dean (1972). Thus, it appears from the model results that the jet transports moisture not only across the equator, but into the interior of Africa. These results disagree with the analysis of the observed 850-mb mean flow over Africa prepared by Ramage and Raman, but agree with Wright and Stubbs.

Figure 6 compares the computed mean sea-level pressure distributions with the observed. The method of conversion of surface to sea-level pressure is discussed in Kasahara and Washington (1971). The July observed means were redrawn from Crutcher and Meserve (1970) and Taljaard *et al.* (1969). The general pattern of low pressure over Iran, Pakistan and

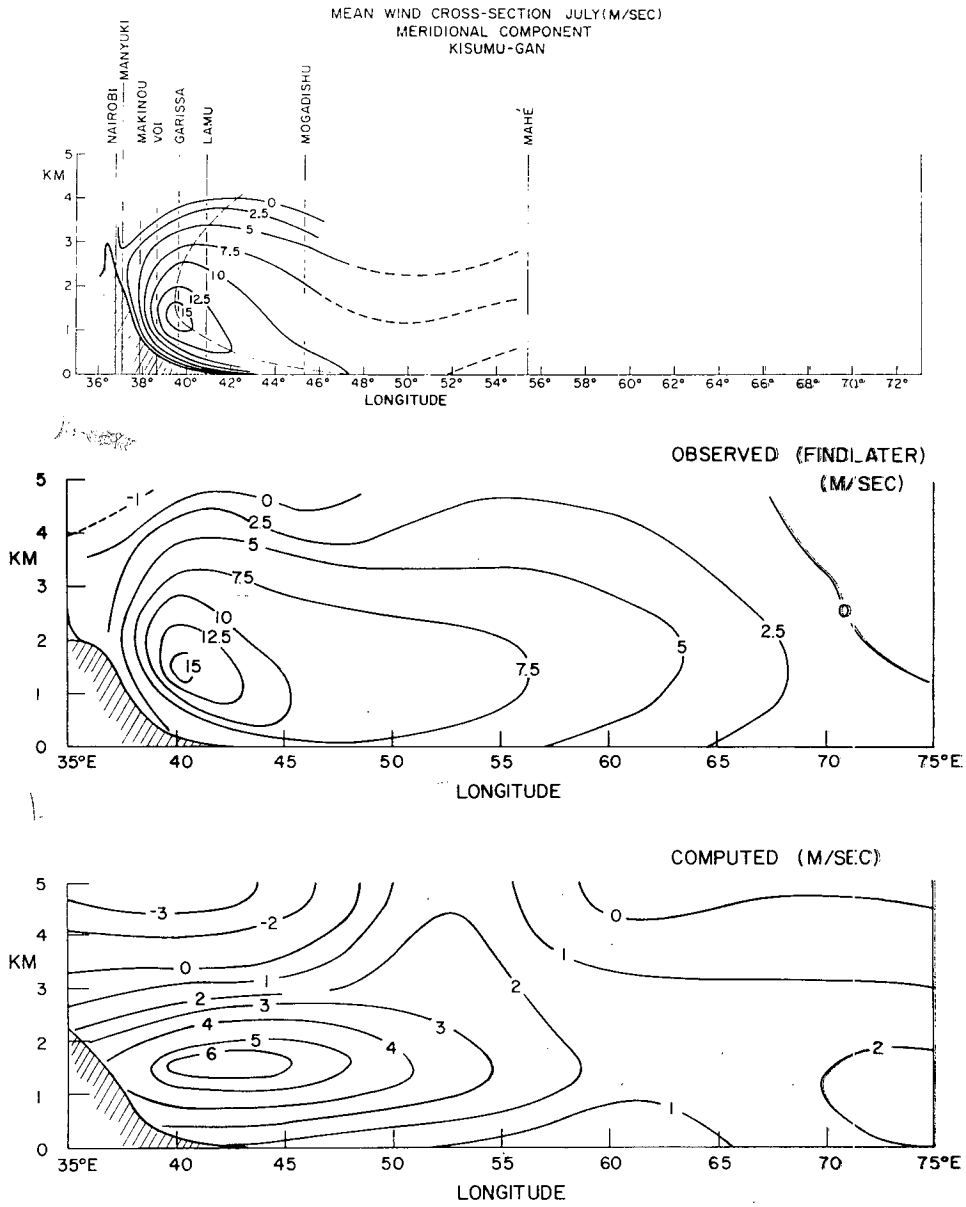

FIG. 4. Cross section of low-level cross-equatorial flow (m s^{-1}) near east coast of Africa; observed from van de Boogaard (private communication) and Findlater (1969).

northern India agrees very well with the observed. Also, the region over the Sahara has relatively low pressure, but not as intense as the observed. The fact that we have high pressure over Kenya and Ethiopia and low pressure northwest of that region is probably closely related to the generation of the Somalian jet referred to in Section 2. Further, the low pressure in the interior of central Africa must also draw air into that region.

It is of interest to inquire about the main dynamics dominating parts of the low-level jet. We compute the geostrophic flow near 10°N by the following equation

$$|V| = \frac{1}{\rho f}\left|\frac{\Delta P}{\Delta N}\right|, \tag{6}$$

where the Coriolis parameter is $f \simeq 2.5 \times 10^{-5}$ s^{-1}, density $\rho \simeq 1.3$ kg m^{-3}, sea-level pressure gradient ΔP 6 hPa(1 mb = 1 hPa) and the distance ΔN for 1100 km. This yields a geostrophic wind approximately 17 m s^{-1} in the low-level jet which is roughly a factor of 2 larger than generated by the model. Presumably, the reason

for the slower wind speed in the model is the effect of surface drag in the model. One aspect that should be pointed out is that from 5° to 10° away from the equator the flow is geostrophic to a large extent and follows the sea-level pressure gradients shown in Fig. 6.

5. Cross sections along 100°E

Another interesting feature of the Asian-African summer monsoon is the formation of the TEJ above a low-level westerly wind maximum in the vicinity of southeast Asia. In Fig. 7, we plot 30-day mean cross-sections of the east-west component of wind u along 100°E. The source for observed winds is Ramage and Raman (1972). We see that the computed pattern successfully simulates the east-west wind reversal. The computed TEJ is weaker and farther south than the observed. The 6-layer version of the NCAR model has a top at 18 km requiring the vertical velocity to be zero at the top. From our results with the stratospheric

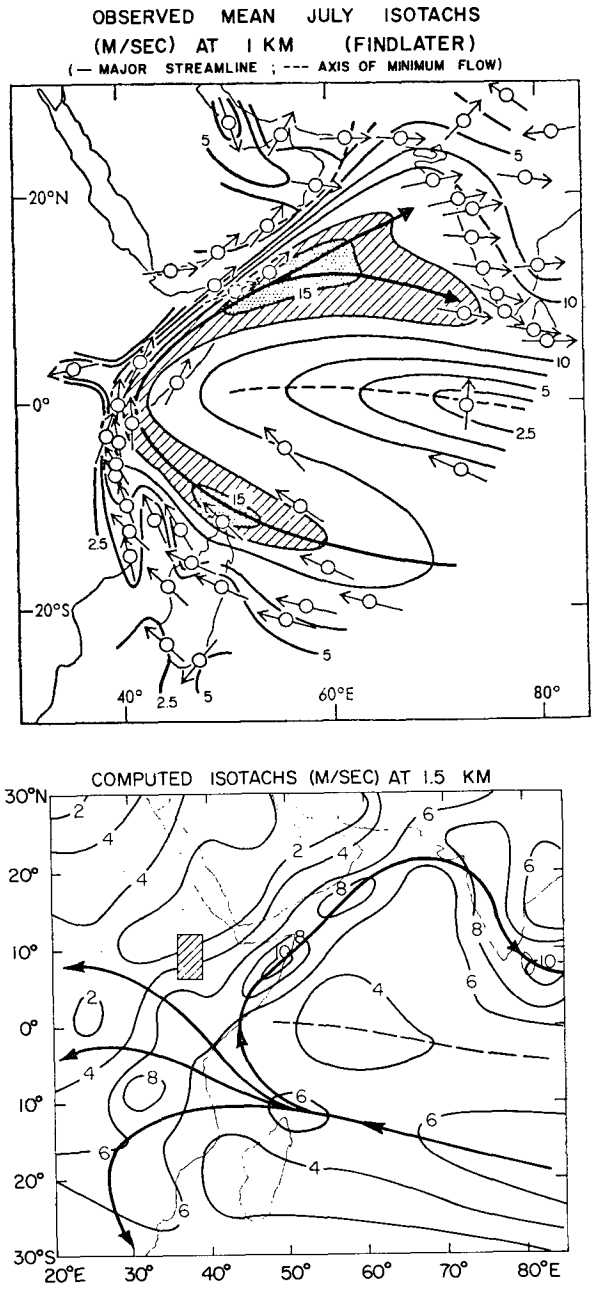

FIG. 5. Horizontal details of the low-level jet; observed (Findlater, 1970) and computed in m s^{-1}.

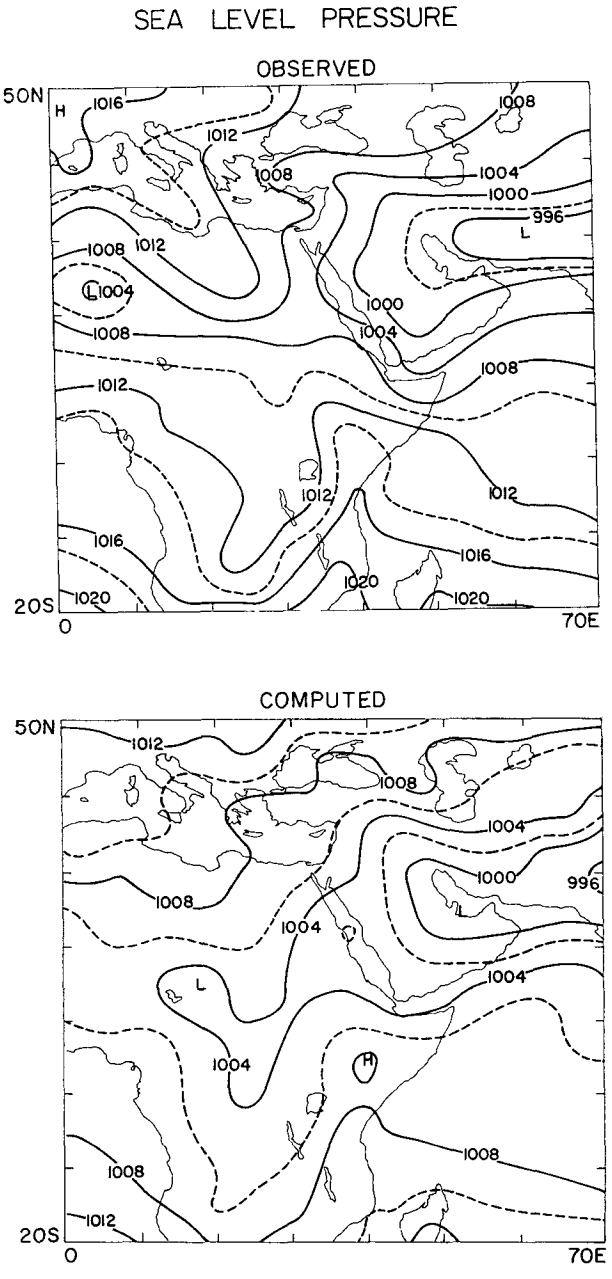

FIG. 6. Observed and computed mean sea-level pressure distributions. Solid contours every 4 mb; dashed contours every 2 mb.

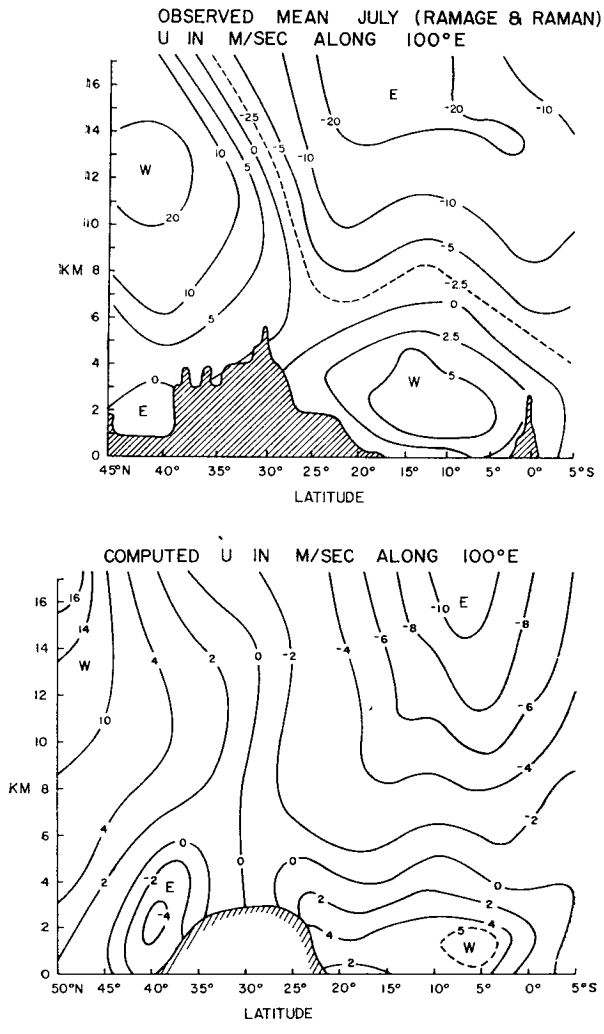

FIG. 7. Mean July observed (Ramage and Raman, 1972) and computed wind speed (m s^{-1}) cross sections along 100°E.

version of the NCAR model (Kasahara *et al.*, 1973), which has a zero vertical velocity boundary condition at 36 km, we find that the tropical tropopause is too warm in a model having a top at 18 km. This defect leads to a weaker-than-normal north-south temperature gradient north of the equator and, in turn, to a weaker-than-normal easterly jet. Another possible reason for this discrepancy with TEJ is the improper location of the precipitation maximum (Section 6). A displaced latent heat source too close to the equator could weaken the latitudinal temperature gradient and then the thermal wind. The zero line between mid-latitude westerlies and easterlies is close to observed. The jet at 45–50°N is too high in the computed case; this shortcoming in the 6-layer model can be corrected by adding more layers in the lower stratosphere as we have shown with our 12-layer model (Kasahara *et al.*, 1973).

The low-level western maximum in Fig. 7 over southeast Asia is the correct speed with the peak about 5° too far equatorward, but too shallow by 1–2 km. This feature of the cross-section is probably affected by the limited horizontal and vertical resolutions of the model.

6. Cloudiness and precipitation

The NCAR model uses a simple linear relationship between cloudiness and local relative humidity (see Kasahara and Washington, 1971, for details). This type of cloudiness formulation works reasonably well in mid-latitudes where layer clouds are more prevalent. However, in the tropics where most clouds are convective, this simple formulation can only delineate the region of a relatively high percentage of cloudiness, especially since essentially all convective clouds derive their moisture from the lower layers of the troposphere. Therefore, a formulation using only *in situ* large-scale relative humidity is bound to be inaccurate in the computation of cloudiness in convective regions, particularly since convective cloudiness results from subgrid-scale processes. We compare in Fig. 8 the computed and observed cloudiness. The simulated cloudiness in tenths is calculated at 3 km and the observed in oktas (eighths) was obtained from Atkinson and Sadler (1970) as an average of three July means. We see that the model-derived cloudiness is underestimated by 0.1–0.2. It is overestimated in the dry regions of southern Africa and the Sahara. Nevertheless, the cloudiness areas over the oceans are in general agreement with observations except over the middle of the Indian Ocean. The ocean maximum coincides with the precipitation pattern discussed later. We also find maximum computed cloudiness over west Africa south of the Sahara. The model computes a relative minimum over the Sahara and Arabia regions, but it fails to find an observed maximum near the Ghat mountain range on the west coast of India. This model deficiency points out a need for improved cloudiness parameterization, especially with orography and convective cloudiness.

Figure 8 compares computed and observed precipitation rates. We redrew the observed prepared by Möller (1951) for easier comparison with the computed and put the contour units in cm d^{-1}. The computed amounts are large over southeast Asia and south of India in relation to the observed of Möller. We appear to have insufficient precipitation in India, partly explained by lack of orographic lifting on the Western Ghats and lack of monsoon depressions which provide a large part of the rainfall over interior India. We note, however, that Manabe *et al.* (1974) recently computed heavy precipitation on the lower tip of India without detailed orography. Over northeast India and the Burma Coast, the computed rainfall rate is in agreement with the observed. It should be pointed out that most of India is relatively dry during the normal monsoon compared with the west coast and northeast regions.

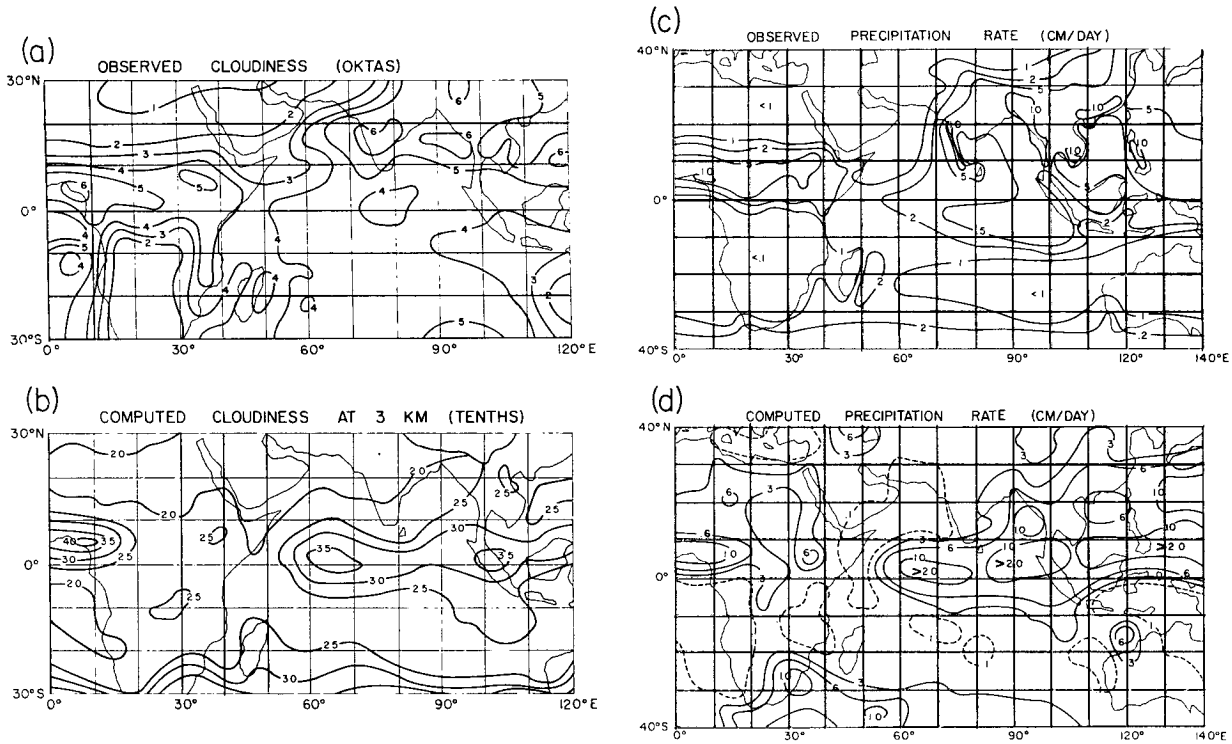

FIG. 8. Comparison of observed and computed cloudiness (oktas and tenths) and precipitation rates (cm d^{-1}): (a) observed cloudiness (Atkinson and Sadler, 1970), (b) computed cloudiness, (c) observed precipitation rate (Möller, 1951), (d) computed precipitation rate.

The model computes an elongated rainbelt across Africa at about 5–10°N which agrees with observed. The western edge of this rainbelt generates much larger precipitation rates than the eastern. The apparent reason is that the low-level winds in western Africa are able to penetrate inland to release their moisture, while in eastern Africa a great deal of the moisture is transported near Africa across the Arabian Sea. Over the Sahara Desert, we obtain minimum rainfall but still much larger than observed. In the region south of the equator, the model computes relatively little rainfall and is in agreement with the observed. Immediately south of the equator, the rainfall amounts are quite small, as they should be in July.

In the vicinity of the mid-Indian Ocean, we obtain very large amounts of rainfall which do not agree with the Möller study in that our maximum is north of the equator and the observed shows a maximum south of the equator. Even though the rainfall pattern is probably closely related to the confluence shown in Fig. 2, the exact reasons for this discrepancy are not known. In a sense, the model appears to form a pattern similar to the "pre-monsoon" intertropical convergence zone often seen in the Indian Ocean north of the equator. Perhaps, with further experimentation with changes in model parameters such as ocean temperature, we could pinpoint the cause of this discrepancy.

7. Conclusions and future plans

We have shown that the NCAR global $2\frac{1}{2}°$ latitude-longitude model is capable of simulating the major mean features of the Asian-African summer monsoon, but with several important discrepancies such as precipitation. To simulate this regional feature of the climate, we must improve the observed data as well as our knowledge of the physical processes. We hope that the proposed GARP Monsoon Experiment (MONEX) will provide the basis for this improved understanding of the Asian-African summer monsoon.

Several experiments are underway which should shed some light on the principal factors controlling the Asian-African monsoon:

a) Removal of orography
b) Changes in western Indian Ocean surface temperatures
c) Simulation of the winter monsoon
d) Seasonal transition from winter to summer monsoon.

These results will be reported elsewhere.

Acknowledgments. We thank G. Williamson for carefully supervising the running of the experiments on the NCAR CDC7600 computer and processing the results. We appreciate the careful drafting of the figures by

G. Meehl and J. Maly. This paper benefited from the constructive comments of D. Baumhefner, A. Kasahara, T. Krishnamurti, R. Madden, C. Newton, T. Schlatter, H. van Loon, H. van de Boogaard, and D. Williamson.

REFERENCES

Abbott, D. A., 1973: Scale interactions of forced quasistationary planetary waves at low latitudes. *Tech. Rept. No. 73-2*, Dept. Meteor., Florida State University, Tallahassee, 190 pp.

Alyea, F. N., 1972: Numerical simulation of an ice age paleoclimate. *Atmos. Sci. Paper No. 193*, Dept. Atmos. Sci., Colorado State University, Fort Collins, 120 pp.

Atkinson, G. D., and J. C. Sadler, 1970: Mean cloudiness and gradient level wind charts over the tropics. Vol. 2, Charts. *Tech. Rept. 215*, U. S. Air Weather Service, 48 pp.

Crutcher, H. L., and J. M. Meserve, 1970: *Selected Level Heights, Temperatures and Dew Points for the Northern Hemisphere.* NAVAIR 50-1C-52 Revised, Naval Weather Service Command, Washington, D. C.

Dean, G. A., 1972: The three-dimensional temperature and wind structure over Africa in 1970. *Tech. Rept. No. 72-3*, Dept. Meteor., Florida State University, Tallahassee, 41 pp. plus 127 figs.

Findlater, J., 1969: Interhemispheric transport of air in the lower troposphere over the western Indian Ocean. *Quart. J. Roy. Meteor. Soc.*, **95**, 400–403.

——, 1970: A major low-level air current near the Indian Ocean during the northern summer: Interhemispheric transport of air in the lower troposphere over the western Indian Ocean. *Quart. J. Roy. Meteor. Soc.*, **96**, 551–554.

——, 1971: Mean monthly airflow at low levels over the western Indian Ocean. *Meteor. Office Geophysical Memoirs No. 155*, 53 pp.

Godbole, R. V., 1973: Numerical simulation of the Indian summer monsoon. *Indian J. Meteor. Geophys.*, **21**, 1–14.

Kasahara, A., and W. M. Washington, 1967: NCAR global general circulation model of the atmosphere. *Mon. Wea. Rev.*, **95**, 389–402.

——, and ——, 1971: General circulation experiments with a six-layer NCAR model, including orography, cloudiness and surface temperature calculations. *J. Atmos. Sci.*, **28**, 657–701.

——, T. Sasamori, and W. M. Washington, 1973: Simulation experiments with a 12-layer stratospheric global circulation model. I. Dynamical effect of the earth's orography and thermal influence of continentality. *J. Atmos. Sci.*, **30**, 1229–1251.

Krishnamurti, T. N., and W. J. Moxim, 1971: On parameterization of convective and nonconvective latent heat release. *J. Appl. Meteor.*, **10**, 3–13.

——, S. M. Daggupaty, J. Fein, M. Kanamitsu, and J. D. Lee, 1973: Tibetan high and upper tropospheric tropical circulations during northern summer. *Bull. Amer. Meteor. Soc.*, **54**, 1234–1249.

Kuo, H. L., 1965: On formation and intensification of tropical cyclones through latent heat release by cumulus convection. *J. Atmos. Sci.*, **22**, 40–63.

Manabe, S., D. G. Hahn, and J. L. Holloway, Jr., 1974: The seasonal variation of the tropical circulation as simulated by a global model of the atmosphere. *J. Atmos. Sci.*, **31**, 43–83.

Möller, F., 1951: Vierteljahrskarten des Niederschlags für die ganze erde. *Petermanns Geogr. Mitt.*, **95**, 1–7.

Murakami, T., R. V. Godbole, and R. R. Kelkar, 1970: Numerical simulation of the monsoon along 80°E. *Proc. Conf. Summer Monsoon of Southeast Asia*, Navy Weather Research Facility, Norfolk, Va., 39–51.

Ramage, C. S., 1971: *Monsoon Meteorology*. New York, Academic Press, 296 pp.

——, and C. R. V. Raman, 1972: *Meteorological Atlas of the International Indian Ocean Expedition, Vol. 2, Upper Air.* National Science Foundation, Washington, D. C., 121 pp.

Taljaard, J. J., H. van Loon, H. L. Crutcher, and R. L. Jenne, 1969: *Climate of the Upper Air: Part 1. Southern Hemisphere. Temperatures, Dew Points, and Heights at Selected Pressures*, Vol. 1. NAVAIR 50-1C-55, Superintendent of Documents, Washington, D. C.

Washington, W. M., 1970: On the simulation of the Indian monsoon and tropical easterly jet stream with the NCAR general circulation model. Preprint Vol., Symp. Trop. Meteor., 2–11 June 1970, Honolulu, Hawaii, Amer. Meteor. Soc., JVI 1–5.

——, 1974: Brief description of NCAR global circulation model. In *Modeling for the First GARP Global Experiment, Rept. No. 14 of GARP Publications Series*. World Meteorological Organization, Geneva, 61–78.

——, and D. P. Baumhefner, 1974: Use of numerical models for tropical climate simulation and forecasting. Preprint Vol., Proc. Symp. Trop. Meteor., 31 January–7 February 1974, Nairobi, Kenya.

——, and A. Kasahara, 1970: A January simulation experiment with the two-layer version of the NCAR global circulation model. *Mon. Wea. Rev.*, **98**, 559–580.

Wright, P. B., and M. W. Stubbs, 1971: Circulation patterns at 850, 700, 500, and 200 millibars over the eastern hemisphere from 40°N to 40°S during May and June. *Meteor. Office Geophysical Memoirs No. 114*, 101 pp.